Recent advances in coherent optical communication

Guifang Li

CREOL, College of Optics & Photonics, University of Central Florida, 4000 Central Florida Boulevard, Orlando, Florida 32816-2700, USA, li@creol.ucf.edu

Received October 19, 2008; revised December 9, 2008; accepted December 11, 2008; posted December 15, 2008 (Doc. ID 102971); published February 11, 2009

Recent progress in coherent optical communication, a field revived by advances in digital signal processing (DSP), is reviewed. DSP-based phase and polarization management techniques make coherent detection robust and practical. With coherent detection, the complex field of the received signal is fully recovered, allowing compensation of linear impairments including chromatic dispersion and polarization-mode dispersion using digital filters. In addition, fiber nonlinearities can also be compensated by using backward propagation in the digital domain.

OCIS codes: 060.4510, 060.1660.

1. Introduction. 281
2. Digital-Signal-Processing-Based Coherent Receiver. 283
   2.1. Digital Carrier-Phase Estimation. 283
      2.1a. Basic Phase Estimation Algorithm. 283
      2.1b. Effect of Additive Noise on Carrier-Phase Estimation. 284
      2.1c. Maximum *a Posteriori* and Decision-Directed Phase Estimation. 285
   2.2. Digital Polarization Demultiplexing. 286
      2.2a. Estimation of Channel Polarization Matrix by Using Training Sequences. 286
      2.2b. Blind Estimation of Channel Polarization Matrix. 288
3. Electronic Compensation of Linear Impairments. 288
   3.1. Dispersion Compensation. 288
   3.2. Polarization-Mode Dispersion Compensation. 289
4. Nonlinearity Compensation. 290
   4.1. Lumped Compensation. 291
   4.2. Distributed Postcompensation of All Fiber Impairments. 291
   4.3. Distributed Cross-Phase Modulation Compensation. 293
   4.4. Distributed Partial Four-Wave Mixing Compensation. 293
   4.5. Computational Requirements for Distributed Nonlinearity Postcompensation. 294
   4.6. Experimental Demonstration of Distributed Nonlinearity Postcompensation. 296

5. High-Spectral-Efficiency Coherent Systems. 297
6. High-Symbol-Rate Coherent Systems. 300
7. Concluding Remarks. 302
Acknowledgments. 304
References. 304

Recent advances in coherent optical communication

Guifang Li

1. Introduction

High-capacity optical transmission has experienced orders of magnitude growth in capacity in the past two decades. The capacity growth has been enabled by key technology breakthroughs such as the erbium-doped fiber amplifier (EDFA), wavelength-division multiplexing (WDM), dispersion compensation and management, and fiber nonlinearity management. In addition, advances in modulation formats led to corresponding increases in fiber transmission capacity in recent years.

In the meantime, spectral efficiency (SE) for fiber-optic transmission has been increasing steadily as well. High SE can be achieved by using modulation formats in which more than 1 bit of information is transmitted in a symbol slot. There are many benefits to employing high-SE modulation formats [1]. High-SE modulation formats can effectively increase the aggregate capacity without resorting to expanding the bandwidth of optical amplifiers. With high-SE formats, the speed of transceiver electronics can be relaxed. High-SE systems are generally more tolerant to chromatic dispersion and polarization-mode dispersion (PMD), since they occupy smaller bandwidths for the same bit rate. Dispersion and PMD tolerance are particularly attractive for high-bit-rate transmission, as dispersion tolerance is reduced by a factor of 4 for an increase in bit per symbol rate by a factor of 2.

Early efforts in achieving high SE used direct detection. A constant-intensity (nonlinearity-tolerant) modulation format that has received great attention is optical differential quaternary phase-shift keying (DQPSK) with differential detection, which can transmit two bits per symbol, corresponding to a theoretical SE of 2 bits/s/Hz [1,2]. To go beyond 2 bit/s/Hz, polarization-division multiplexing (PDM) has been suggested to further increase SE in combination with DQPSK [3]. However, since the state of polarization of the light wave is not preserved during transmission, dynamic polarization control is required at the receiver to recover the transmitted signals. An alternative approach is to use independent intensity modulation on top of DQPSK, resulting in eight-level amplitude-phase-shift keying [4]. Of course, eight-level amplitude-phase-shift keying is not a constant-intensity modulation format. References [5–7] proposed and demonstrated two constant-intensity direct-detection modulation formats, namely, optical differential eight-level phase-shift keying (8PSK) [5,6] and differential Jones vector-shift keying [7].

In the past few years, research in high-capacity transmission has shifted to

coherent detection, in part to achieve high SE. Coherent detection was the subject of intensive research in the 1980s because of its high sensitivity [8,9]. One of the main reasons that coherent optical communication was abandoned, starting in the early 1990s, was the invention of EDFAs. Preamplified receivers using EDFAs achieve sensitivity within a few decibels of that of coherent receivers, thus making coherent detection less attractive, considering its complexity.

In coherent optical communication, information is encoded onto the electrical field of the light wave; decoding entails direct measurement of the complex electrical field. To measure the complex electrical field of the light wave, the incoming data signal (after fiber transmission) interferes with a local oscillator (LO) in an optical 90° hybrid as schematically shown in Fig. 1. If the balanced detectors in the upper branches measure the real part of the input data signal, the lower branches, with the LO phase delayed by 90°, will measure the imaginary part of the input data signal. For reliable measurement of the complex field of the data signal, the LO must be locked in both phase and polarization with the incoming data.

Phase and polarization management turned out to be the main obstacles for the practical implementation of coherent receivers. The state of polarization of the light wave is scrambled in the fiber. Dynamic control of the state of polarization of the incoming data signal is required so that it matches that of the LO. Each dynamic polarization controller is bulky and expensive [10]. For WDM systems, each channel needs a dedicated dynamic polarization controller. The difficulty in polarization management alone severely limits the practicality of coherent receivers. Phase locking is challenging as well. All coherent modulation formats with phase encoding are usually carrier suppressed. Therefore, conventional techniques such as injection locking and optical phase-locked loops cannot be directly used to lock the phase of the LO. Instead, decision-directed phase-locked loops must be employed [11,12]. At high symbol rates, the delays allowed in the phased-locked loop are so small that it becomes impractical [12].

So what are the reasons that coherent optical communication is making a comeback, and why is it possible now? The answer lies in advances in digital signal processing (DSP). Both phase and polarization management can be realized in the electrical domain by using DSP. Moreover, coherent detection in conjunction with DSP enables compensation of fiber-optic transmission

Figure 1

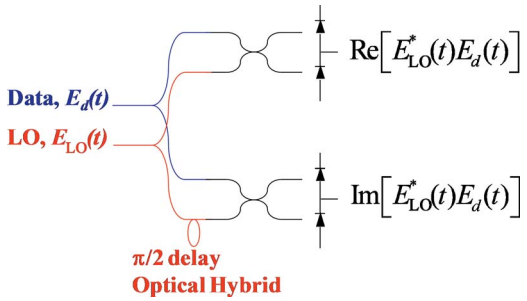

Schematic of a coherent receiver.

impairment, opening up new possibilities that will likely shape the future of optical transmission technology. This paper is organized as follows. Section 2 describes coherent receivers using DSP for phase and polarization management. Section 3 presents compensation of linear impairments in fiber transmission using coherent detection and DSP. Section 4 details recent activities in compensation of nonlinear impairments in fiber transmission. Section 5 discusses high-SE transmission using coherent modulation and detection. Section 6 explores approaches for high-symbol-rate coherent transmission. Concluding remarks are given in Section 7.

2. Digital-Signal-Processing-Based Coherent Receiver

2.1. Digital Carrier-Phase Estimation

2.1a. Basic Phase Estimation Algorithm

Phase locking in the hardware domain can be replaced by phase estimation in the software–DSP domain. An algorithm for DSP-based phase estimation is schematically shown in Fig. 2 [13,14]. A quadrature phase-shift keying (QPSK) signal is used as an example, in which the signal can be represented as

$$E(t) = A \exp\{j[\theta_s(t) + \theta_c(t)]\}, \tag{1}$$

where the optical carrier phase $\theta_c(t)$ is the phase of the transmitter laser referenced to the LO and the data phase takes on four values, $\theta_s = 0, \pm\pi/2, \pi$. To estimate the carrier phase θ_c by using DSP, the received signal has to be detected coherently to obtain its real and imaginary parts. This is done by using a LO and an optical 90° hybrid as shown in Fig. 1 [15]. The complex received signal is then digitized by using analog-to-digital conversion (ADC) and processed in the software domain by using DSP. When the received signal is raised to the fourth power as shown in Fig. 2, we obtain

$$A^4 \exp[j\{4\theta_s(t) + 4\theta_c(t)\}] = A^4 \exp[j\{4\theta_c(t)\}], \tag{2}$$

because $\exp[j4\theta_s(t)] = 1$, i.e., the power operation strips off the data phase. The carrier phase can then be computed and subtracted from the phase of the received signal to recover the data phase as shown in Fig. 2. Such a feed-forward phase estimation scheme lends itself well to real-time digital implementation [16]. Figure 2, however, is an idealization where no additive noise is present

Figure 2

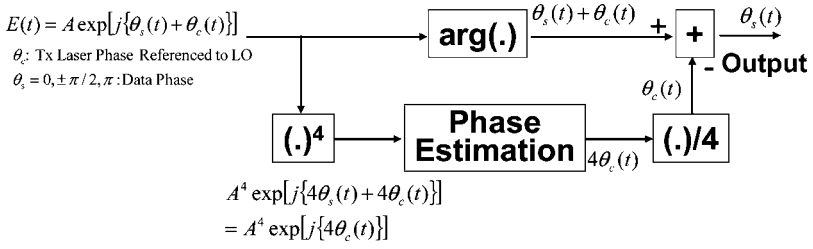

Schematic of the phase estimation algorithm for QPSK.

in the received signal. In realistic systems, the received signal will contain noise dominated by either ASE–LO beat noise (where ASE is amplified spontaneous emission) or shot noise of the LO. In the presence of these additive noises, digital carrier-phase estimation must be adapted to manage these noises.

2.1b. Effect of Additive Noise on Carrier-Phase Estimation

In reality, each complex sample at the receiver includes additive noise and, again using QPSK as an example, can be written as

$$r_k = \exp[j\{\theta_s(k) + \theta_c(k)\}] + n_k, \tag{3}$$

where k denotes the kth symbol, the amplitude of the received signal has been normalized, and n_k is the additive noise, which is assumed to be a complex zero-mean Gaussian distribution random variable characterized with a variance σ_n^2. Raising the received QPSK signal to the fourth power yields

$$r_k^4 = \exp\{j4\,\theta_c(k)\} + 4\exp\{j[3\,\theta_s(k) + 3\,\theta_c(k)]\}n_k + o(n_k^2) \tag{4}$$

and, in the small-angle approximation,

$$\arg(r_k^4) = 4\,\theta_c(k) + \delta(\theta_c)n_k + o(n_k^2), \tag{5}$$

where $\delta(\theta_c)$ is a small quantity. It is apparent that the phase estimate is no longer accurate in the presence of additive noise. The phase estimation error will be of the order of $\delta(\theta_c)n_k/4$, which is inversely proportional to the signal-to-noise ratio.

A method to reduce the effect of additive noise on phase estimation error is to average the estimated phase over a sequence of symbols by filtering the per-symbol phase estimate through an equal-tap-weight transversal filter [16,17]:

$$\theta_{c,\mathrm{est}} = \frac{1}{4}\arg\left\{\sum_{k=1}^{N_b} r_k^4\right\}. \tag{6}$$

This implementation is referred to as block-window filtering as sequences of data are processed in blocks. Assuming that the carrier phase is constant over the sequence of symbols, the variance of the phase estimation error due to additive noise is then reduced by a factor equal to the symbol sequence length N_b. The filtering process itself introduces an error in phase estimation, as the carrier phase is actually not constant owing to the finite beat linewidth of the transmitter and LO lasers. This error thus increases with N_b. A trade-off between these two effects dictates that the tap number for the additive noise filter must be optimized. In the case of block-window filtering, the carrier-phase estimate is the same for the entire sequence of symbols. In [14], it was shown through a series of approximations that the phase estimation error for QPSK using a block window can be modeled as a zero-mean Gaussian random variable with a variance depending on the beat linewidth, electrical signal-to-noise ratio, and block size. The equal-tap-weight filter can also be implemented by using gliding window filtering [18].

Since the phase estimate is forced in value in the range $-\pi/4 \le \theta_{c,\mathrm{est}}(k) \le \pi/4$, there is a fourfold phase ambiguity. It is important to differentially precode data to avoid error propagation. In addition, to avoid cycle slips when

the difference in the carrier-phase estimates between adjacent blocks is $>\pi/4$ or $<-\pi/4$, the two data symbols at the boundary of the two blocks should be shifted or rotated appropriately after differentially decoding. Details of this method, as well as its real-time implementation using parallel processing, can be found in [16].

Because the laser phase noise is a Wiener process and the additive noise is Gaussian, the Wiener filter, in fact, provides the best phase estimation according to estimation theory [19]. The detailed derivation can be found in [20]. The Wiener filter can make an estimate $\theta_{c,\mathrm{est}}(k)$ based on all samples up to and including r_k, in which case the filter is referred to as the zero-lag Wiener filter. Alternatively, the Wiener filter can make an estimate $\theta_{c,\mathrm{est}}(k)$ based on all samples up to and including r_{k+D}, where D is a positive integer, in which case the filter is referred to as the finite-lag Wiener filter. The finite-lag Wiener filter has been shown to perform better because it estimates the phase both forwards and backwards in time. The z transfer function of the zero-lag and finite-lag Wiener filters are given by [20]

$$H_{\mathrm{ZL}}(z)=\frac{1-\alpha}{1-\alpha z^{-1}}, \tag{7}$$

$$H_{\mathrm{FL}}(z)=\frac{(1-\alpha)\alpha^{D}+(1-\alpha)^{2}\Sigma_{k=1}^{D}\alpha^{D-k}z^{-k}}{1-\alpha z^{-1}}, \tag{8}$$

from which the coefficients of the finite impulse response (FIR) filters can be obtained accordingly. The parameter α depends on the variance of the phase noise and additive noise and is given by

$$\alpha=\frac{M^{2}\sigma_{w}^{2}+2\sigma_{q}^{2}-M\sigma_{w}\sqrt{M^{2}\sigma_{w}^{2}+4\sigma_{q}^{2}}}{2\sigma_{q}^{2}} \tag{9}$$

for an M-ary phase-shift keying signal. In Eq. (9), σ_q^2 is the variance of the noise term $\delta(\theta_c)n_k$ in Eq. (5) and $\sigma_w^2=2\pi\Delta\nu T$, where $\Delta\nu$ is the beat linewidth of the transmitter and LO lasers and T is the symbol period. It should be pointed out that the additive noise filter can also be realized by using a gliding window filter, which might be more compatible with real-time implementation.

In the above discussion, we have assumed that the frequency of the LO is the same as the transmitter laser. This requirement is not necessary, since the frequency difference between the transmitter and LO lasers can also be estimated in the digital domain. This type of coherent receiver is called the intradyne receiver. Algorithms for frequency estimation for intradyne receivers and their real-time implementation can be found in [18,21].

2.1c. Maximum a Posteriori and Decision-Directed Phase Estimation

The best estimate of carrier phase given the observed values r_k is the maximum *a posteriori* estimate [20,22]. The conditional probability density function of the received signal, conditioned on the transmitted signal s_k, is given by

$$p(r_k|s_k,\theta_c(k))=\frac{1}{\pi\sqrt{2\sigma_n^2}}\exp\left(-\frac{|r_k-s_k e^{j\theta_c(k)}|^2}{2\sigma_n^2}\right). \tag{10}$$

The maximum *a posteriori* phase estimate is the sequence of values $\hat{\mathbf{s}}_k$ and $\hat{\boldsymbol{\theta}}_c$ that maximizes the probability function

$$(\hat{\mathbf{s}}, \hat{\boldsymbol{\theta}}_c) = \max_{\mathbf{s}, \boldsymbol{\theta}_c} \left\{ \prod \frac{1}{\pi\sqrt{2\sigma_n^2}} \exp\left(- \frac{|r_k - s_k e^{j\theta_c(k)}|^2}{2\sigma_n^2} \right) \right\} p(\mathbf{s}) p(\boldsymbol{\theta}_c), \tag{11}$$

where we have used the fact that the sequence of $\hat{\mathbf{s}}_k$ and $\hat{\boldsymbol{\theta}}_c$ are statistically independent. Since the probability density function $p(\mathbf{s})$ is known *a priori* and $\theta_c(k)$ is a Wiener process, taking the logarithm of Eq. (11) yields

$$(\hat{\mathbf{s}}, \hat{\boldsymbol{\theta}}_c) = \max_{\mathbf{s}, \boldsymbol{\theta}_c} \sum_k \left(- \frac{|r_k - s_k \exp(i\theta_c(k))|^2}{2\sigma_n{}^2} - \frac{(\theta_c(k) - \theta_c(k-1))^2}{2\sigma_w{}^2} \right). \tag{12}$$

Equation (12) is a joint estimation of the carrier phase and data. As a result, it is nearly impossible to solve for $\hat{\mathbf{s}}_k$ and $\hat{\boldsymbol{\theta}}_c$ by using any method that is suitable for a real-time operation. However, the maximization in Eq. (12) can be performed offline, and the results can be used as the baseline to evaluate the effectiveness of different carrier-phase estimation algorithms.

For real-time implementation, it is necessary to estimate the carrier phase independently from data recovery to reduce the computational load. The power-law carrier-phase estimation method discussed in Subsections 2.1 and 2.2 is effective for phase-shift keying signals because the operation strips off data, making the carrier-phase estimation independent of data. Another approach is either data-assisted or decision-directed carrier-phase estimation [22]. In data-assisted carrier-phase estimation, training symbols at the beginning are used to estimate carrier phase, which is assumed to be slowly varying and thus provides a good estimate for the data that follow the training symbols. In decision-directed carrier-phase estimation [20,22], the recovered data are assumed to be correct, which is true for systems operating a low bit error rate (BER). The recovered data can then remodulate the incoming signal to extract the carrier phase.

2.2. Digital Polarization Demultiplexing

In conventional approaches, polarization demultiplexing is accomplished by using dynamic polarization controllers and polarization splitters. Just as optical phase locking can be replaced by phase estimation through DSP, polarization demultiplexing can also be achieved in the DSP domain.

2.2a. Estimation of Channel Polarization Matrix by Using Training Sequences

It is possible to demultiplex PDM signals by using electronics rather than optics [18,23]. The key is to observe the analogy between PDM and multiple-input–multiple-output (MIMO) antenna wireless communications. As a result, algorithms for wireless MIMO channel estimation can be readily applied to polarization demultiplexing in optical polarization MIMO [23].

The schematic of an optical polarization MIMO system is shown in Fig. 3. In the transmitter, two synchronous data are modulated in orthogonal polarizations. The modulation format can be amplitude and/or phase modulation. E_x and

Figure 3

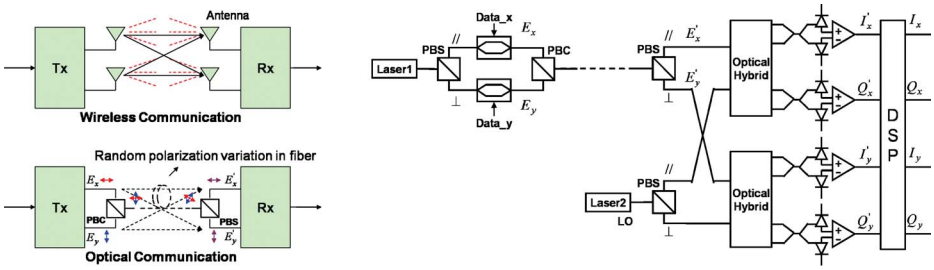

(a) (b)

(a) Analogy between wireless MIMO and optical PDM and (b) Schematic of an optical polarization MIMO system. PBS, polarization beam splitter; PBC, polarization beam combiner [23].

E_y are the complex representation of the modulated signal in the parallel and perpendicular polarization state. After transmission through fiber, the polarization of the light wave is usually not preserved. For an arbitrarily orientated polarization beam splitter, the received signal, E_x' or E_y', contains significant cross talk between the original signals in the two orthogonal polarization states. The output electrical field can be related to the input electrical field by

$$\begin{pmatrix} E_x' \\ E_y' \end{pmatrix} = L \begin{pmatrix} J_{xx} & J_{xy} \\ J_{yx} & J_{yy} \end{pmatrix} \begin{pmatrix} E_x \\ E_y \end{pmatrix} = JL \begin{pmatrix} E_x \\ E_y \end{pmatrix}, \tag{13}$$

where L is a real scalar describing the optical loss from the input to the output, and the polarization change due to fiber is described by a unitary Jones matrix J. Equation (13) describes a two-input and two-output MIMO system, as shown in Fig. 3(a). Since J is a unitary matrix, this MIMO system, in theory, can transmit two synchronous channels without any penalty [24]. Because of environment variations, the polarization of the light wave in fiber generally drifts with time. The rate of this polarization drift is generally much slower than the transmission data rate. Therefore, the system can be designed to estimate the Jones matrix J for the entire frame by using a training sequence in the preamble of each frame to remove polarization cross talk. Various channel estimation algorithms can be used to estimate J. Considering the high data rate used in optical communications, the least-mean-squares algorithm was chosen in [25] for its simplicity. Matrix J can be estimated by using the following iterative algorithm:

$$J_i = J_{i-1} + \mu \left[\begin{pmatrix} E_x' \\ E_y' \end{pmatrix}\Bigg|_i - J_{i-1} L \begin{pmatrix} E_x \\ E_y \end{pmatrix}\Bigg|_i \right] L \begin{pmatrix} E_x \\ E_y \end{pmatrix}\Bigg|_i^T,$$

$$i \geq 0, \quad J_{-1} = \text{initial guess}, \tag{14}$$

where μ is a positive step size, i is the training sequence label, and L can be obtained from the received average power. Since E_x' and E_y' are generally complex, 90° optical hybrids are used to simultaneously measure the in-phase I_x' and I_y' and quadrature Q_x' and Q_y' components. The inverse of estimated J can then be applied to the received signals to recover the transmitted data I_x, I_y,

Q_x and Q_y. Since J is a unitary matrix, its inversion and conjugate transpose are identical. In optical polarization MIMO systems, the received signal polarization estimation and tracking are performed by DSP algorithms, and no optical dynamic polarization control is required at the receiver.

2.2b. Blind Estimation of Channel Polarization Matrix

It is possible to estimate the Jones matrix of the transmission system without relying on a training sequence if there exist statistical properties of the transmitted symbols that can be exploited. In particular, for PDM systems using constant-intensity modulation formats such as QPSK, the Jones matrix can be estimated using the fact that the modulus of the received signal should be constant [26]. Without loss of generality, let us assume that the constant modulus is unity. An estimate of the Jones matrix is obtained by minimizing the mean squared errors $\langle \varepsilon_{x,y}^2 \rangle$ of the quantities $\varepsilon_{x,y} = 1 - |E'_{x,y}|^2$. In order to do so, the gradient of the mean squared error with respect to the appropriate elements of the Jones matrix should vanish, i.e.,

$$\frac{\partial \varepsilon_x^2}{\partial J_{xx}} = 0, \quad \frac{\partial \varepsilon_x^2}{\partial J_{xy}} = 0, \quad \frac{\partial \varepsilon_y^2}{\partial J_{yx}} = 0, \quad \frac{\partial \varepsilon_y^2}{\partial J_{yy}} = 0. \tag{15}$$

To obtain the estimate of the channel Jones matrix, it is initialized as an identity matrix. Subsequently, the matrix elements are updated by using the stochastic gradient algorithm [27] as follows:

$$J_{xx} \rightarrow J_{xx} + \mu \varepsilon_x E''_x E'^*_x,$$

$$J_{xy} \rightarrow J_{xy} + \mu \varepsilon_x E''_x E'^*_y,$$

$$J_{yx} \rightarrow J_{yx} + \mu \varepsilon_y E''_y E'^*_x,$$

$$J_{yy} \rightarrow J_{yy} + \mu \varepsilon_y E''_y E'^*_y,$$

where * denotes complex conjugate, (E''_x, E''_y) is the demultiplexed optical field, and μ is a positive convergence parameter.

3. Electronic Compensation of Linear Impairments

The main driver for coherent optical communication is the possibility to compensate for transmission impairments by using DSP [28]. This is possible only when both the phase and the magnitude of the complex field of light are detected. All linear impairments in fiber-optic transmission systems can potentially be compensated.

3.1. Dispersion Compensation

Dispersion in optical fiber is an all-pass filter on the electric field of the light wave, given by a complex transfer function in the frequency domain:

Figure 4

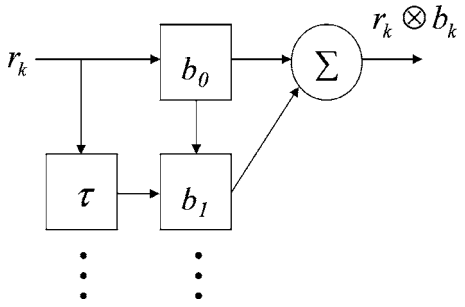

Schematic of an FIR digital filter for compensation of chromatic dispersion.

$$H_f(\omega) = \exp\left\{ j \cdot \frac{\lambda_0^2 Dz}{4\pi c} \cdot \omega^2 \right\}. \tag{16}$$

With coherent detection, the effect of dispersion can be reversed or compensated by a filter with a transfer function given by $\tilde{H}_f(\omega) = H_f^*(\omega)$ [29–31]. Such a filter can be realized by using a FIR filter, as shown in Fig. 4, with coefficients given by the discrete inverse Fourier transform of $b_n = (1/N)\Sigma_{k=0}^{N-1} H_f^*(\omega_k) e^{j\cdot\omega_k \cdot n}$.

Alternatively, the dispersion compensation filter in the digital domain can be realized by using an infinite impulse response filter [29], which was shown to be more computationally efficient but requires buffering.

3.2. Polarization-Mode Dispersion Compensation

The concept of polarization MIMO can be extended to describe PMD by a time-dependent 2×2 channel matrix [26,30],

$$J(t) = \begin{pmatrix} J_{xx}(t) & J_{xy}(t) \\ J_{yx}(t) & J_{yy}(t) \end{pmatrix}, \tag{17}$$

where J_{ij} denotes the response at the ith output polarization due to an impulse applied at the jth input polarization of the fiber. Figure 5 describes a receiver

Figure 5

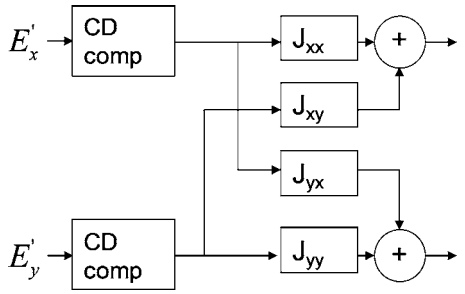

Receiver architecture for polarization demultiplexing and PMD compensation, after [26].

architecture for chromatic dispersion and PMD compensation. The input signals E_x' and E_y' are complex signals coherently detected on the two polarizations. The fixed chromatic dispersion compensating FIR filter (CD comp) is the same for both polarizations and is used to compensate for the majority of the chromatic dispersion. The adaptive FIR filters undo polarization rotation and PMD in a butterfly arrangement.

Savory *et al.* [26] demonstrated PDM QPSK transmission at 10 Gsymbols/s over 6400 km of fiber, compensating all linear impairments by using DSP as outlined above. Figure 6 shows the constellation diagrams of the two polarizations after transmission. In particular, the stochastic gradient constant modulus algorithm [27], which does not need training bits, was used for polarization division demultiplexing. It should be noted that polarization-dependent loss makes the channel polarization matrix nonunitary, leading to penalties in electronic polarization demultiplexing and complication in blind channel polarization matrix estimation.

4. Nonlinearity Compensation

The degree to which fiber impairments are compensated ultimately determines the transmission capacity of fiber optic transmission systems. Nonlinear impairments can be compensated by using electronics or DSP as long as they are deterministic, because propagation in optical fiber is well described mathematically by the nonlinear Schrödinger equation (NLSE). Nonlinear impairments can be precompensated at the transmitter or postcompensated at the receiver. Because of fiber dispersion and nonlinearity, the received signal is different from the transmitted signal. To ensure that the received signal is identical to the transmitted signal, virtual fibers, with signs of dispersion and nonlinearity opposite to those of the physical transmission fiber, must be added in the DSP domain in the transmission system. In the precompensation of nonlinear impairments, the virtual fiber is placed between the input data stream and the optical in-phase–quadrature modulator so that the signal is predistorted by the virtual fiber while being compensated through the real transmission fiber. Several electrical precompensation schemes have been demonstrated to compensate for chromatic dispersion or nonlinearity in

Figure 6

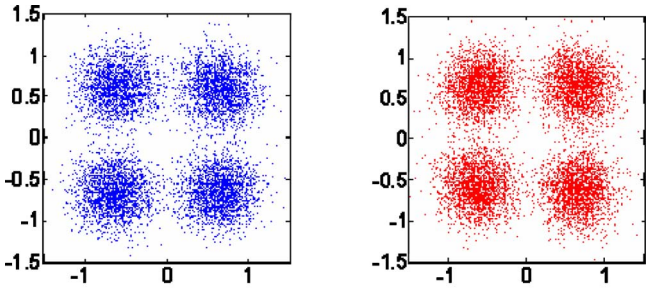

Constellation diagrams for the (a) *x* and (b) *y* polarization at the receiver after 6400 km of transmission with an estimated BER $= 2.4 \times 10^{-3}$ [26].

single-channel or WDM systems [32–36]. In the postcompensation of nonlinear impairments, the virtual fiber is placed after coherent detection so that the signal is distorted in the real transmission fiber while being compensated through the virtual fiber. In this section we focus mainly on postcompensation, which offers great flexibility, since adaptive compensation can be incorporated into this scheme. Postcompensation using coherent detection and DSP has been shown to be very effective in chromatic dispersion compensation (CDC) [28] and intrachannel nonlinearity compensation [37]. We recently reported postcompensation of both linear and nonlinear impairments in WDM transmission [38].

4.1. Lumped Compensation

Lumped nonlinearity compensation can be used to potentially compensate self-phase modulation (SPM) that is due to deterministic data patterns such as in quadrature amplitude modulation transmission or nondeterministic effects that are due to the Gordon–Mollenauer effect by applying an intensity-dependent phase modulation. SPM due to data patterns could be compensated at the receiver but is better compensated at the transmitter because the applied phase modulation will be free of additive noise accumulated in transmission. Compensation of the Gordon–Mollenauer effect can be achieved only at the receiver by applying a phase modulation proportional to the intensity of the received signal. This can be achieved in the optical domain [39] but has recently been demonstrated in the DSP domain. It should be pointed out that the lumped compensation of SPM works well only for low-dispersion or dispersion-compensated transmission lines. It is straightforward to show that, on average, lumped compensation of the Gordon–Mollenauer effect can reduce the nonlinear phase noise by 6 dB [17].

4.2. Distributed Postcompensation of All Fiber Impairments

In [38], transmission of WDM signals (the total number of channels is C) by using postcompensation of all linear and nonlinear fiber impairments is investigated, as opposed to precompensation [35]. The schematic of the transmission system is shown in Fig. 7(a), where postcompensation is performed in the digital domain after coherent detection. After transmission, the received signals are mixed in a 90° optical hybrid with a set of LOs, of which C LOs are aligned at the center of the WDM channels. Additional LOs are aligned with other four-wave mixing (FWM) components outside the WDM band. The in-phase and quadrature components of each WDM channel are obtained by balanced photodetectors. Analog-to-digital conversion is followed by DSP to achieve postcompensation and data recovery.

The backward propagation compensation scheme for a multispan fiber link is shown in Fig. 7(b), where G is the optical gain of the linear optical amplifiers in the fiber link and $E(t)$ and $E'(t)$ are the electrical fields of the received signal and the compensated signal, respectively. Let $\hat{E}_m$ be the envelope of the optical field for the mth channel, where $m \in I$, $I=\{1,2,\ldots,C\}$. The full optical field can be expressed as

$$E=\sum_m E_m=\sum_m \hat{E}_m \exp(im\Delta\omega t), \tag{18}$$

where $\Delta f=\Delta\omega/2\pi$ is the channel spacing. The reconstructed total field in Eq. (18) will be used as the input for backward propagation in order to

Figure 7

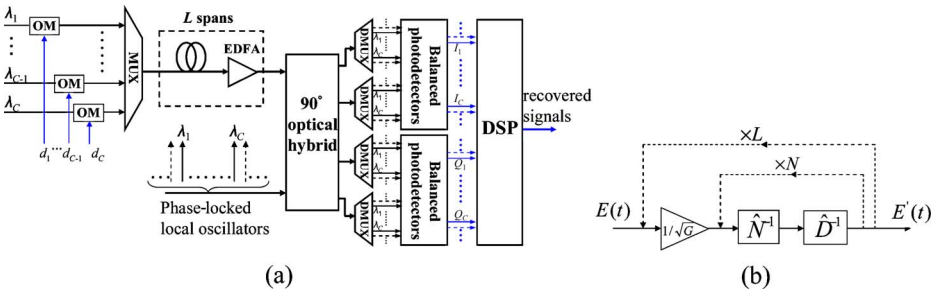

(a) Architecture of WDM transmission with fiber dispersion and nonlinearity compensation using coherent detection and DSP. Optical path, black; electrical path, blue; OM, optical modulator. (b) Backward propagation for a multispan fiber link. L, span number; N, step number per span [38].

compensate all deterministic transmission impairments. The total-field backward propagation equation, i.e., TNLSE, is given by [9]

$$\frac{\partial E}{\partial z} = (\hat{N}^{-1} + \hat{D}^{-1})A, \tag{19}$$

where $\hat{N}^{-1}$ and $\hat{D}^{-1}$ are inverse nonlinear and differential operators, respectively, and are given by [40]

$$\hat{N}^{-1} = i\gamma'|E|^2, \quad \hat{D}^{-1} = -\frac{i\beta_2'}{2}\frac{\partial^2}{\partial t^2} + \frac{\beta_3'}{6}\frac{\partial^3}{\partial t^3} - \frac{\alpha'}{2}. \tag{20}$$

Here γ', β_2', β_3', and α' are the fiber nonlinear coefficient, first- and second-order group-velocity dispersion, and loss coefficient. When these parameters are chosen to be exactly the negative of the values for the transmission fiber, nonlinearity and dispersion can be compensated through backward propagation. The NLSE is most commonly solved by using the split-step Fourier method. In this approach, each span of fiber is divided into N sections, and $\hat{N}^{-1}$ and $\hat{D}^{-1}$ are implemented sequentially. To facilitate real-time implementation, the dispersion or differential operator ($\hat{D}^{-1}$) can be realized by using an FIR filter instead of a Fourier transform, which has been shown to achieve acceptable accuracy [41].

Numerical simulations of a 10×10 Gbit/s binary phase-shift keying (BPSK) WDM system near 1550 nm with a channel spacing of 20 GHz using postcompensation were carried out in [38]. Forward propagation of WDM signals over dispersion-shifted fiber was simulated by using VPI Transmission Maker. The fiber loss, dispersion, dispersion slope, and nonlinearity at 1550 nm are 0.2 dB/km, 0 ps/km/nm, 0.04 ps/km/nm^2, and 1.8 W^{-1}/km, respectively. The EDFAs are set to power mode with a noise figure of 5 dB. Both transmitter lasers and LOs have a linewidth of 2 MHz. The optical demultiplexers have a 3 dB bandwidth of 19 GHz, and the photodetectors have an electrical bandwidth of 9 GHz.

The back-to-back electrical eye-diagram of the fifth WDM channel is shown in Fig. 8(a). The rails on eyes are from linear cross talk due to the small channel

Figure 8

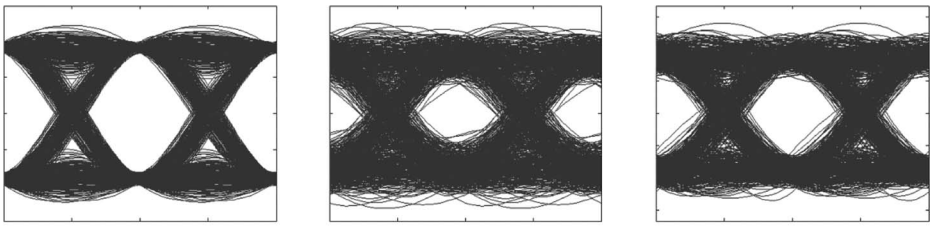

Eye diagrams of the fifth WDM channel: (a) at back-to-back, (b) after 500 km transmission over DSF without ENLC, (c) after 500 km transmission over DSF with ENLC [38].

spacing. Figures 8(b) and 8(c) show the eye diagrams of the received signals after 500 km transmission over DSF without and with electronic nonlinearity compensation (ENLC), respectively. The Q factor of the eye diagram in Fig. 8(b) is about 6. It is clearly seen that the eye diagram in Fig. 8(c) is more open because of nonlinearity compensation. In fact, the Q factor reaches $Q \approx 6$ after 800 km transmission over DSF with ENLC. This implies that the transmission distance with digital nonlinearity compensation is increased by 60% in this preliminary study.

4.3. Distributed Cross-Phase Modulation Compensation

If XPM is the dominant nonlinearity effect, the effect of FWM can be omitted in backward propagation. Substituting the total field E given by Eq. (18) into Eq. (19), expanding the $|E|^2$ term, and neglecting all FWM terms yields [42,43]

$$C[\hat{E}_m] = -\frac{\partial \hat{E}_m}{\partial z} + \frac{\alpha}{2}\hat{E}_m + K_{1m}\frac{\partial \hat{E}_m}{\partial t} + K_{2m}\frac{\partial^2 \hat{E}_m}{\partial t^2} + K_{3m}\frac{\partial^3 \hat{E}_m}{\partial t^3} + i\gamma\left(\sum_q^C |\hat{E}_q|^2 - |\hat{E}_m|^2\right)\hat{E}_m = 0, \tag{21}$$

with $k_{1m} = m\beta_2\Delta\omega - m^2\beta_3\Delta\omega^2/2$, $k_{2m} = i\beta_2/2 - m\beta_3\Delta\omega/2$, $k_{3m} = -\beta_3/6$. The above system of coupled NLSEs describes the backward evolution of the baseband WDM channels where dispersion, SPM, and XPM are compensated. The above equations can also be solved in the digital domain by the well-known split-step Fourier FIR method (SSFM) [42].

4.4. Distributed Partial Four-Wave Mixing Compensation

As will be described below, FWM compensation requires a remarkable amount of calculations compared with XPM compensation only. However, for low-dispersion regimes, FWM can substantially impair the signal because of an increased degree of phase matching. Partial compensation of FWM can be implemented by using an enhanced system of coupled equations, where

FWM interaction is compensated on a channel-by-channel basis, by considering the nonlinear mixing of the neighboring channels. As a result, Eq. (21) can be now rewritten as

$$EC[\hat{E}_m] = C[\hat{E}_m] + F_{3m} + F_{5m} = 0, \tag{22}$$

where

$$F_{3m} = 2\hat{E}_{m+1}\hat{E}_{m-1}\hat{E}_m^*,$$

$$F_{5m} = \hat{E}_{m+1}^2\hat{E}_{m+2}^* + \hat{E}_{m-1}^2\hat{E}_{m-2}^* + 2\hat{E}_{m-1}\hat{E}_{m+1}\hat{E}_{m+1}^* + 2\hat{E}_{m+1}\hat{E}_{m-2}\hat{E}_{m-1}^* + 2\hat{E}_{m+2}\hat{E}_{m-2}\hat{E}_m^*. \tag{23}$$

In Eq. (22), F_3 represents the FWM interaction of two neighboring channels, whereas F_5 includes the interaction of four neighboring channels. Since the effective bandwidth for FWM compensation is small, both sampling rate and step size remain the same as for the XPM compensation case. Even though only a small number of FWM terms are considered in Eq. (22), these terms are highly phase matched. Hence, improved results are expected without significant increase of computational resources. The SSFM implementation of Eq. (22) can be implemented in a perturbative manner, where the nonlinear operator (see for example [42,43]) for the kth step is approximated by

$$\hat{E}_m^k = \hat{E}_m^{k-1}\exp(i\gamma|\hat{E}_m^{k-1}|^2 h) + h(F_{3m}^{k-1} + F_{5m}^{k-1}), \tag{24}$$

where h is the SSFM step size.

4.5. Computational Requirements for Distributed Nonlinearity Postcompensation

Two fundamental parameters have to be considered when addressing the computational requirements for TNLSE or coupled NLSE approaches. These parameters are the sampling rate and the SSFM step size.

For postcompensation by using TNLSE, each detected channel has to be upsampled so that the bandwidth of the reconstructed full optical field is wide enough to avoid aliasing of newly generated FWM products. Specifically, the sampling rate for each symbol for using TNLSE is

$$S_{\mathrm{TNLSE}} = 2C\Delta f/B, \tag{25}$$

where B is the symbol rate per channel. The above formula forces the sampled bandwidth to be twice the optical bandwidth. On the other hand, XPM compensation using coupled NLSEs does not create new frequency components. Hence, a proper backward propagation can be performed by using only two samples per symbol.

The number of operations is also proportional to the number of steps and hence inversely proportional to the step size. The SSFM accuracy depends fundamentally on the mutual influence of dispersion and nonlinearity within the step length. Owing to the nature of the dispersion and nonlinearity operators, the step size has to be chosen such that (1) the nonlinear phase shift is

small enough to preserve the accuracy of the dispersion operation and (2) the optical power fluctuations due to dispersion effects are small enough to preserve the accuracy of the nonlinear operation.

One way to set the upper bound for the step size is to identify the characteristic physical lengths, which correlate the optical field fluctuations with the propagation distance. Three physical lengths are of interest here, namely, the nonlinear length L_{nl}, the walk-off length L_{wo}, and the FWM length L_{fwm}. The nonlinear and walk-off lengths can be defined, for a multichannel system, as follows:

$$L_{\mathrm{nl}} = \frac{1}{\gamma P_T \dfrac{2C-1}{C}}, \quad L_{\mathrm{wo}} = \frac{1}{2\pi|\beta_2|(C-1)\Delta f B}, \tag{26}$$

where $P_T = \Sigma_m |E_m|^2$ is the total launched power and, again, B is the symbol rate (effectively the inverse of the pulse width). The nonlinear length has been defined as the length after which an individual channel achieves a 1 rad phase shift due to SPM and XPM. The walk-off length is defined as the distance after which the relative delay of pulses from the edge channels is equal to the pulse width. The above characteristic lengths are well known [44] and widely used to qualitatively describe the optical field behavior through fiber propagation. However, when FWM is considered, the nonlinear and walk-off lengths are not enough to qualitatively identify the range where the **fastest** field fluctuations take place. For this purpose, the total optical field should be rewritten as $E = \Sigma_m E_m \exp(ik_m z)$, where k_m is the linear propagation constant of the mth channel. By following the same procedure as for Eq. (21), the nonlinear term, now including FWM, can be expressed as follows for the mth channel:

$$-i\gamma\left(2\sum_{q\in I}|E_q|^2 - |E_m|^2\right)E_m - i\gamma\left[\sum_{[rslm]\in I} E_r E_s E_l^* \exp(i\delta k_{rslm} z)\right], \tag{27}$$

with the conditions $l = r+s-m$, $[m,r,s] \in I$, and $r \neq s \neq m$. The first condition neglects fast time-oscillating terms (frequency matching). The second condition forces the newly generated waves to lay within the WDM band. Finally, the third condition excludes SPM and XPM terms. δk_{rslm} is the phase-mismatch parameter, given by

$$\delta k_{rslm} = k_r + k_s - k_l - k_m = \frac{1}{2}\beta_2 \Delta\omega^2 [r^2 + s^2 - (r+s-m)^2 - m^2]. \tag{28}$$

To identify the **fastest** z fluctuations for the mth channel, set $r = 1$ and $s = C$, corresponding to the indexes of the edge channels. Maximizing Eq. (28) leads to the expression for the maximum phase-mismatch:

$$\delta k_{\max} = \frac{1}{4}|\beta_2|(C-1)^2 \Delta\omega^2. \tag{29}$$

The above expression leads to the following definition for the FWM length:

$$L_{\mathrm{fwm}} = \frac{1}{\pi^2 |\beta_2|(C-1)^2 \Delta f^2}. \tag{30}$$

The above expression represents the length after which the argument of the **fastest** FWM term is shifted by 1 rad; hence, it can be understood as the distance after which power fluctuations due to FWM start to take place. The definition of the FWM length assumes that the FWM-induced variations on a given channel are governed by the linear (dispersive) phase mismatch. However, nonlinearity also contributes to the overall phase mismatch through SPM and XPM. This contribution is relevant only in high-power regimes, and it is not expected to play a role in the analysis of fiber transmission. The SSFM step size will be correlated with the minimum characteristic length involved in each case; thus, for the compensation of SPM and XPM effects via coupled equations, the step size is limited by the walk-off length, whereas the FWM length will be the parameter limiting the step size for the total-field NLSE. For WDM systems, the nonlinear length is longer than the FWM and walk-off lengths for the typical launch powers of interest in communications. In [43], a detailed analysis of the step size requirements for both XPM and XPM plus FWM compensation is performed, showing that a correct FWM postcompensation requires remarkably smaller step sizes compared with XPM compensation, which translates into a higher computational load. In addition, phase locking of the LO is not necessary for the coupled NLSEs for either XPM compensation or XPM plus partial FWM compensation.

Preliminary results also show that distributed nonlinearity postcompensation is robust against small fluctuations or uncertainties of transmission fiber parameters. In addition, distributed nonlinearity postcompensation can be employed for fibers with PMD and PDM transmission in fibers with PMD. The additional computation required to compensate for PMD is minimal, although per-span PMD monitoring is required. It should be pointed out that the discussions in this subsection and the preceding Subsections 4.2 and 4.3 also apply to distributed precompensation [36].

4.6. Experimental Demonstration of Distributed Nonlinearity Postcompensation

The first experimental demonstration of distributed nonlinearity postcompensation was reported in [45]. Three distributed-feedback lasers were used as WDM carriers as shown in Fig. 9. The center channel (λ_C) and two adjacent channels (λ_R and λ_L) are BPSK modulated by using Mach–Zehnder modulators (MZMs) driven at 6 Gbaud by a pattern generator (PG) with a pseudorandom bit sequence of length $2^{23}-1$. A symbol rate of 6 Gbaud was chosen to fit three WDM channels within the real-time oscilloscope (RTO) double-sided analog bandwidth of 24 GHz. The WDM channels are tightly spaced at 7 GHz, which was found to give the lowest linear cross talk because of the nonideal waveforms [46]. Polarization controllers (PCs) were placed at the appropriate locations to ensure that all the channels are copolarized. The launch power in each channel was equalized by using optical attenuators.

A total launching power (P_L=6 dBm) into the optical fiber was set by using an EDFA, calibrated to the insertion losses associated with the recirculating loop components. The recirculating loop consists of two nonzero dispersion-shifted fiber spools, with a combined length of 152.82 km. The fiber parameters are α=0.2 dB/km, β_2=−4.9 ps^2/km, and γ_{NL}=1.9/km/W. A phase diversity receiver is used to beat the transmitted optical signal with the LO tuned to the center channel. The real-time oscilloscope RTO was used

Figure 9

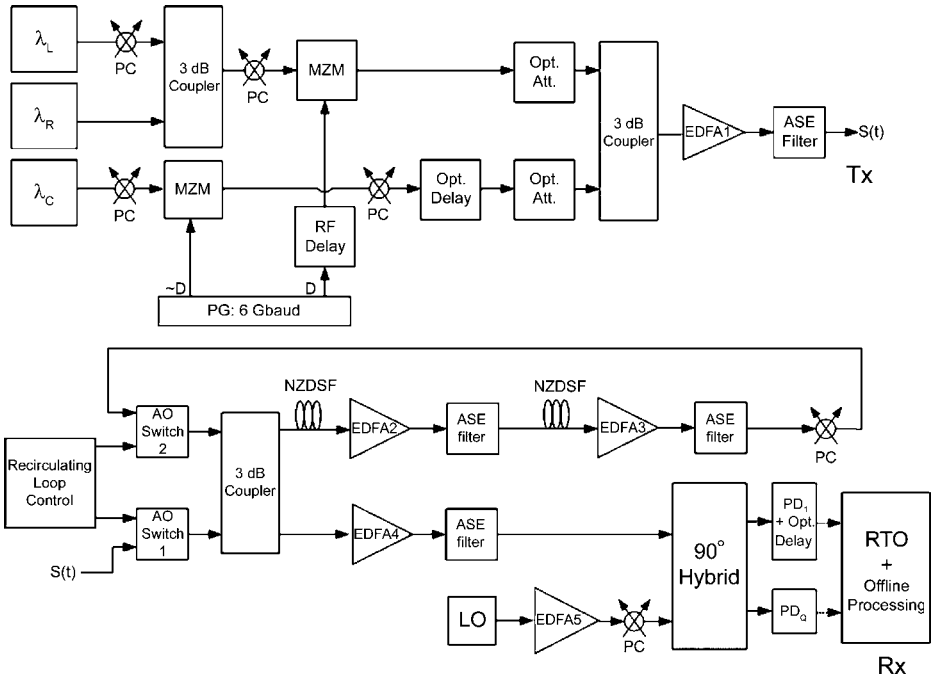

Experimental setup for OWDM [45].

to digitize the two signal quadratures at 40 Gsamples/s. DSP was performed offline. The dispersion length is $[\beta_2(24\ \text{GHz})^2]^{-1} \cong 355$ km. Considering the effects of SPM and XPM and neglecting loss, the nonlinear length can be defined as $[\gamma_{\text{NL}}(5/3)P_{\text{eff}}]^{-1} \cong 282$ km, where $P_{\text{eff}} = P_L \int_0^{z_{\text{span}}} e^{-\alpha x} dx / z_{\text{span}} = 0.28 P_L$ accounts for the fiber loss. As discussed in [47], for the FWM effects in a C channel system to be accounted for properly, the step size should be smaller than $[\pi \Delta f^2 |\beta_2| (C-1)^2]^{-1} \cong 105$ km. Both spools used are shorter than the characteristic lengths discussed above. So a step size that matches each spool (approximately 75 km) was used in backward propagation. After employing backward propagation and proper WDM filtering [46], eye diagrams of the received signal were obtained.

To evaluate its effectiveness, the distributed backward propagation nonlinearity compensation method was compared with other compensation techniques, including (1) CDC only and (2) lumped compensation, which includes CDC followed by a single nonlinear compensating operation consisting of a phase shift proportional to the signal power. Figure 10 shows eye diagrams for the back-to-back, CDC, lumped nonlinearity compensation, and distributed nonlinearity compensation after 760 km nonzero dispersion-shifted fiber transmission. Distributed nonlinearity compensation provides a clearly open eye.

5. High-Spectral-Efficiency Coherent Systems

High SE can effectively increase the aggregate capacity without resorting to expanding the bandwidth of optical amplifiers. There are two ways to increase SE in optical transmission for which coherent detection is ideally suited.

Figure 10

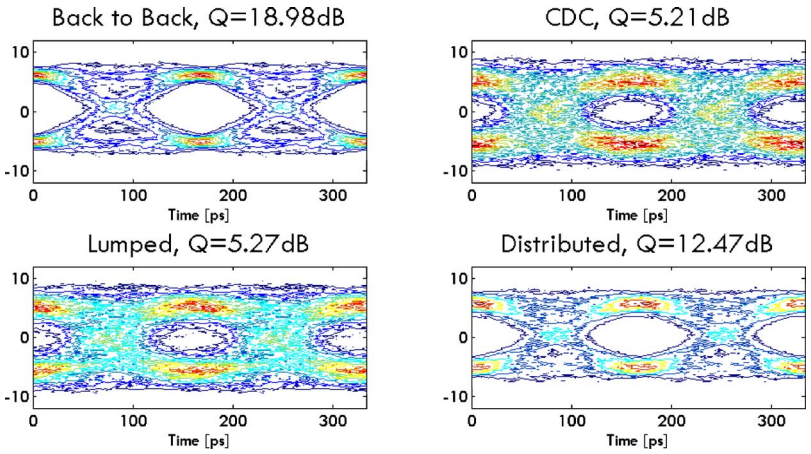

Eye diagrams for (top left) back-to-back and after 760 km with compensation, using (top right) CDC, (bottom left) lumped, and (bottom right) distributed [45] compensation.

One way is to use advanced modulation formats so that each symbol transmits multiple bits of information. Using carrier-phase estimation, 8PSK has been demonstrated in [48,49]. QPSK and 8PSK with PDM were demonstrated in [48,50]. Richer constellation has been demonstrated by using conventional heterodyne phase-locked loop (PLL) detection [51]. It is expected that DSP-based coherent transmission of high-order quadrature amplitude modulation will soon follow.

The other way to increase SE is to pack WDM channels closer together. An advantage of coherent detection is its inherent ultranarrow optical filtering capability useful for dense WDM. This is because channel filtering can be implemented in the electrical domain after coherent detection. In general, reducing channel spacing in a WDM system is expected to lead to increased penalty due to linear cross talk where the spectra of adjacent channels start to overlap. Orthogonal WDM (OWDM) via coherent detection with channel spacing equal to the symbol rate was recently proposed and demonstrated for achieving the highest possible SE [46,52]. To see how linear cross talk can be eliminated in OWDM, let the electrical field of the transmitted optical signal of the WDM system be given as

$$s(t) = \sum_{k=1}^{C} \sum_{q=0}^{\infty} a_{k,q} g(t - qT) e^{j\omega_k t}, \tag{31}$$

where C, $a_{k,q}$, $g(t)$, T, and ω_k are the total number of optical channels, the qth information symbol of the kth channel, pulse shape, and angular frequency of the kth channel carrier, respectively. At the coherent receiver, the transmitted signal is beat with the LO. Noise $n(t)$ (expressed in baseband) is added to the signal by the communications channel, and then it is detected by a coherent receiver. The output signal from the receiver is

$$r(t) = (s(t)e^{-j\omega_{\mathrm{LO}}t} + n(t)) \otimes h(t), \tag{32}$$

where $h(t)$ is the net receiver impulse response, composed of the impulse response of the receiver front end combined with an equalization filter, and $n(t)$

is the additive noise. ω_{LO} refers to the effective LO frequency, given by the actual LO frequency together with any adjustment applied in the digital domain. For OWDM, the channel spacing is chosen such that

$$\omega_k - \omega_{k-1} = 2\pi/T. \tag{33}$$

Assuming that $g(t)$ is a perfectly square pulse (of width T) and $h(t)$ is the same square pulse (the matched filter), Eq. (32) becomes, for two channels spaced by $2\pi/T$, where $\omega_{LO}=\omega_1$,

$$r(t) = \sum_{q=0}^{\infty} \int_0^T (a_{1,q} g(t-\tau-qT) + a_{2,q} g(t-\tau-qT) \exp\left(j\frac{2\pi}{T}t\right) \exp\left(-j\frac{2\pi}{T}\tau\right) d\tau,$$

$$r(t) = \sum_{q=0}^{\infty} a_{1,q} g \otimes h(t-qT). \tag{34}$$

The second channel is extinguished by convolution with the receive filter; therefore there is no linear cross talk from the adjacent channels. The principle of OWDM is fundamentally the same as in orthogonal frequency-division multiplexing (OFDM) in the electrical or optical communication systems [53–56]. The difference is that orthogonality is maintained among optical carriers in OWDM, while orthogonality is maintained among RF subcarriers in OFDM, and these subcarriers are modulated onto an optical carrier.

An experiment, shown in Fig 11(a), demonstrating the principle of OWDM using coherent detection was reported in [46]. The center channel (ω_C) is BPSK modulated by using a Mach–Zehnder modulator (MZM) driven at 6 Gbaud by a pattern generator (PG). Two adjacent channels (ω_R and ω_L) are also modulated and combined with the center channel. Note that the adjacent channels have synchronized symbol times but decorrelated data content compared with the center channel. Noise is loaded by combining the three modulated channels with the output of several cascaded EDFAs with no input, inducing ASE. A 90° hybrid and real-time oscilloscope (RTO) were used to coherently detect and sample the noise-loaded signal. The LO frequency was set to match ω_C. The obtained samples were processed offline. The decision-threshold Q factor as a function of channel spacing is shown in Fig. 11(b). When the channel spacing is much tighter than the symbol rate, a large penalty is incurred. This penalty is reduced as the channel spacing grows, up to an optimal point. Note that this shift in optimum channel spacing to a higher value than the symbol rate is due to the finite rise time of the pulse (stemming from limited bandwidth). Increasing the channel spacing even further actually increases the penalty. But from a certain channel spacing onward the channels are spaced enough that the spectral overlap is diminished and the Q factor levels off. Also shown in Fig. 11(b) are the simulation results when three and five WDM channels are present. There is a slight penalty (0.8 dB) when five channels are considered, which arises because the next-nearest neighbors have a small spectral overlap with the center channel.

Figure 11

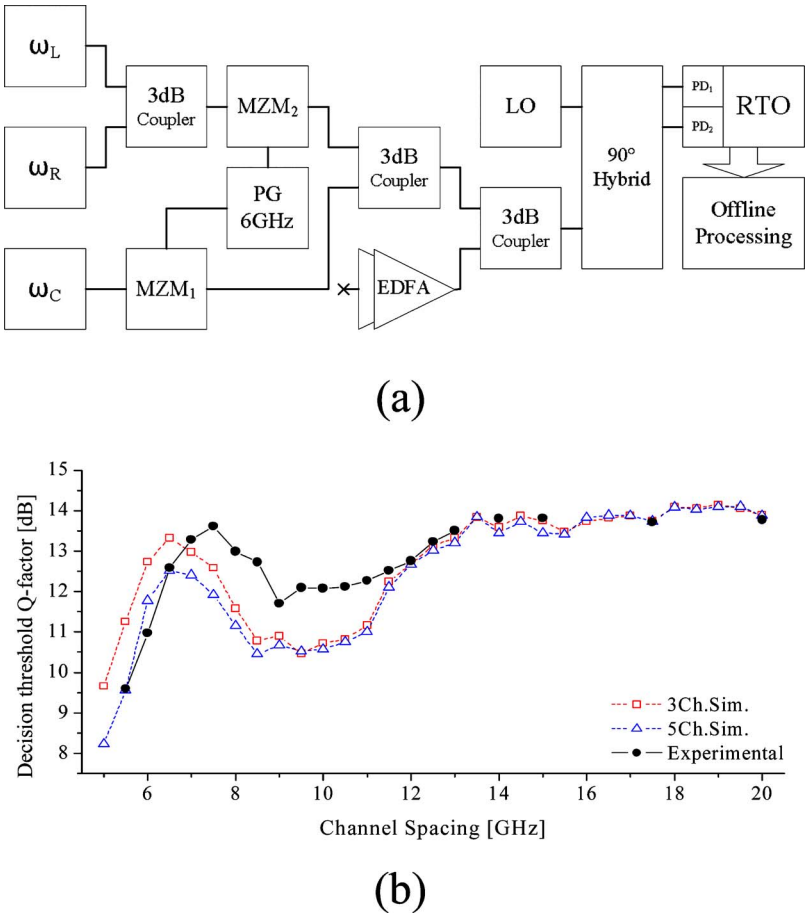

(a) OWDM experimental setup; (b) Q factor versus channel spacing [46].

6. High-Symbol-Rate Coherent Systems

Looking ahead of the landscape for DSP-based coherent optical communication, one of the possible bottlenecks for realizing future high-symbol-rate transmission systems is the ADC technology. Coherent optical time-domain sampling (COTDS) [57] can be a potential solution, as it can be used to demultiplex the waveform into tributaries slow enough for electronic ADC. Figure 12(a) shows the schematic for a 1×2 COTDS setup where two samples

Figure 12

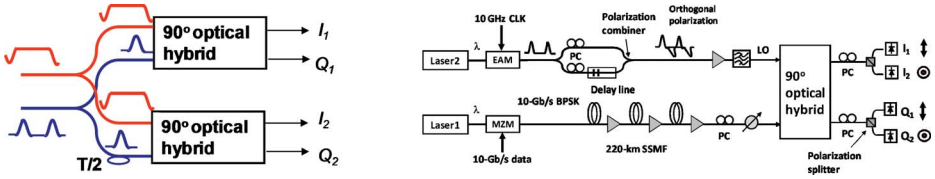

(a) Schematic and (b) experimental setup for COTDS [58].

from one symbol are demultiplexed into two data streams at half the symbol rate.

A 1×2 COTDS experiment was carried out to demonstrate 10 Gbit/s BPSK transmission and dispersion compensation [58]. The setup is shown in Fig. 12(b). A 10 Gbit/s BPSK signal after 220 km standard single-mode fiber (SSMF) [$D=17$ ps/(km nm)] transmission was coherently detected by using COTDS, and the dispersion was electronically compensated. For dispersion compensation, a sampling rate of 20 Gsamples/s is required for 10 Gbit/s signal. In this experiment, the sampling rate ADC was set at 10 Gsamples/s, and two COTDS pulse trains with repetition rate of 10 GHz were used as LOs to perform parallel optical sampling. The wavelengths of the transmitter and the LO laser were 1550 nm, and their frequency difference was tuned to be as small as possible. An electroabsorption modulator was modulated by a 10 GHz clock at a proper bias point to achieve a pulse train with a pulse width around 20 ps. The pulse train was then divided into two by a 50 ps relative delay. Polarization manipulations were used so that only one 90° optical hybrid is required, and the two orthogonal LO pulse trains beat with the received signal independently. The outputs of the hybrid were separated by two polarization splitters and then detected by four detectors with a 12 GHz bandwidth. A real-time digital oscilloscope was used as ADC and sampled at 10 Gsamples/s. The signal power launched into SSMF was 0 dBm, and the EDFAs had noise figures around 5 dB. The total LO power was set to be −2.6 dBm.

The relative phase φ_{rel} between the two LO channels should be stable and known to perform electronic dispersion compensation and phase estimation properly. In this experiment, we estimated the relative phase in postprocessing. Once φ_{rel} is obtained, it can be compensated because it varies slowly. We chose consecutive "1"s and "0"s, which had small phase change between adjacent sample points even after transmission, to calculate the phase difference between the two LO pulse trains. The corresponding sample points of these consecutive symbols in the two tributaries should have almost the same phase, so they could be used to calculate φ_{rel}. This algorithm was demonstrated for the 220 km SSMF transmission experiment. After the relative phase estimation, we performed offline signal processing and BER measurement from recorded data by applying electronic dispersion compensation and phase estimation after transmission. The accumulated dispersion value was 3740 ps/nm. The block size for the phase estimation was 15. A gliding window was used for each symbol in phase estimation [58]. We measured the eye diagram and BER of the 10 Gbit/s BPSK signals when the 1×2 COTDS was used. For comparison, we also conducted an experiment using a CW LO and 20 Gsample/s ADC to electronically sample the signals. The eye diagrams before and after electronic dispersion compensation and phase estimation of the two schemes are shown in Fig. 13 ($P_s=-19$ dBm). It can be seen that COTDS worked well for coherent detection and dispersion compensation.

Without the requirement for phase continuity between COTDS tributaries, the setup can be used for optical time-domain demultiplexing. Reference [59] demonstrated optical time-domain demultiplexing of a 320 Gbit/s QPSK signal with a digital coherent receiver having an optical time-domain demultiplexing function.

Figure 13

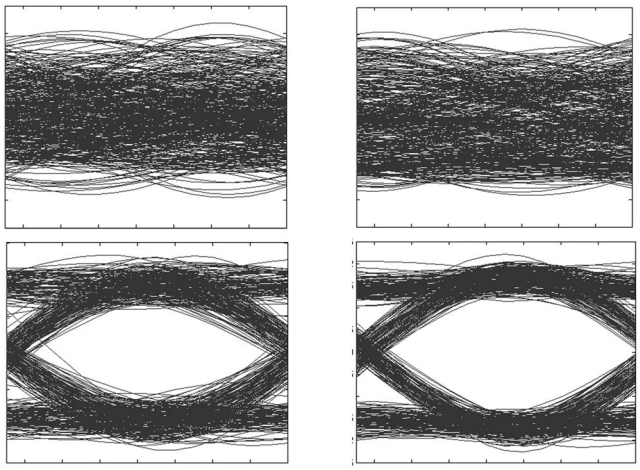

Eye diagrams before and after dispersion compensation and phase estimation using (a) optical sampling and 10 Gsample/s ADC and (b) CW LO and 20 Gsample/s ADC [58].

7. Concluding Remarks

It is an exciting time for the field of optical communication, as it is witnessing the rebirth of coherent optical communication. Preamplified optical communication systems made possible by the invention of EDFAs have been the mainstay for research and commercialization since the demise of coherent optical communication in the early 1990s. Advances in integrated circuits and DSP technologies have fortunately brought coherent optical communication to the forefront again. In fact, recent developments in DSP-enabled coherent optical communication mirror advances in the field of RF–wireless communication. However, DSP-enabled coherent optical communication is advancing at a much faster pace. Techniques that were developed for RF–wireless communication over the past few decades have been applied to coherent optical communication over the past few years, including real-time implementations [50,60,61]. Reference [50] describes a real-time coherent receiver that performs dispersion compensation, polarization demultiplexing, and PMD compensation, carrier-phase estimation, and data recovery for a PDM QPSK system operating at 10 Gsymbol/s (40 Gbits/s). Figure 14 shows the photograph of the CMOS ASIC (application-specific integrated circuit) for the receiver, which executes 12×10^{12} operations per second. Progress in ASICs such as this provides optimism for more advanced signal processing functions in coherent optical communication, including nonlinearity compensation.

The capacity of a communication channel is the product of the spectral bandwidth W and the maximal SE. According to the Shannon capacity formula for the additive white Gaussian noise channel with an average power constraint $W \log_2(1+S/N) W \log_2(1+S/N)$, with S being input light power and N the power of ASE noise in the system. However, the fiber (channel) is not

Figure 14

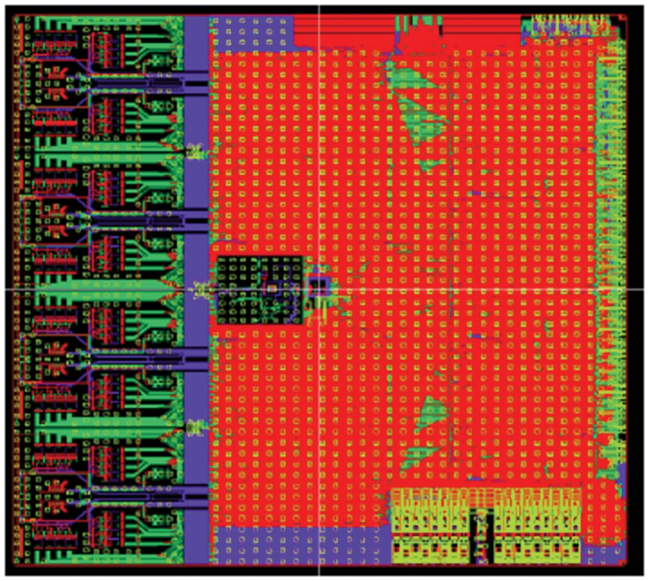

Photograph of a CMOS ASIC coherent receiver for PDM QPSK with four 20 Gsample/s ACDs and 12×10^{12} operations per second [50].

linear. The amount of nonlinear noise (SPM, XPM, and FWM) increases faster than the signal power. The effect is a saturation and eventual decline of SE as a function of input signal power for a WDM system using on–off keying [62], in complete contrast with the linear channel case.

With nonlinearity compensation using the backward propagation method, all deterministic nonlinear effects including SPM, XPM, and FWM due to data modulation can potentially be fully compensated. The fundamental SE limit will then be bounded by ASE at low input power densities in the same way as above and will be bounded by ASE-seeded nonlinearities at high input power densities. These nonlinearities include not only ASE-seeded nonlinearities in the transmission fibers but also nonlinearities induced by ASE–LO beat noise (in the coherent receivers) in the virtual back propagation fiber. This new fundamental SE limit with coherent detection and nonlinearity compensation has yet to be determined. In a practical system, the deterministic nonlinearities cannot be compensated exactly because of quantization noise and also finite step size. It would be interesting to obtain a lower bound on the practical capacity limits as a function of ADC resolution and step size by using the semianalytical method as in [62]. ADC resolution and step size (proportional to number of operations) both affect system cost.

There has been an exponential growth in research activities in coherent optical communication since 2004. The author apologizes that only a small fraction of the work was referenced in this article. The readers should refer to the proceedings of the Optical Fiber Communication Conference and the European Conference on Optical Communication since 2004 as well as relevant journals to gain a complete picture of the state of the art in coherent optical communication.

Acknowledgments

I thank Seb Savory of University College London and Kim Roberts of Nortel for permission to use their figures ([6] and [50], respectively). I acknowledge the technical contributions related to this manuscript from former members of my group, including Cheolhwan Kim, Yan Han, Zhihong Li, Inwoong Kim, and Kevin Croussore, and current members of my group, including Xiaoxu Li, Gilad Goldfarb, Eduardo Mateo, Likai Zhu, Fatih Yaman, and Xiabo Xie. The additional, current group members also provided assistance in preparing this manuscript. This work was supported in part by the Defense Advanced Research Projects Agency (DARPA) under contract DAAD1702C0097.

References

1. R. Griffin and A. C. Carter, "Optical differential quadrature phase-shift key (oDQPSK) for high capacity optical transmission," in *Optical Fiber Communications Conference*, A. Sawchuk, ed., Vol. 70 of OSA Trends in Optics and Photonics (Optical Society of America, 2002), paper WX6.
2. T. Tokle, C. R. Davidson, M. Nissov, J. X. Cai, D. Foursa, and A. Pilipetskii, "6500 km transmission of RZ-DQPSK WDM signals," Electron. Lett. **40**, 444–445 (2004).
3. P. S. Cho, G. Harston, C. J. Kerr, A. S. Greenblatt, A. Kaplan, Y. Achiam, G. Levy-Yurista, M. Margalit, Y. Gross, and J. B. Khurgin, "Investigation of 2-b/s/Hz 40-gb/s DWDM transmission over 4×100 km SMF-28 fiber using RZ-DQPSK and polarization multiplexing," IEEE Photon. Technol. Lett. **16**, 656–658 (2004).
4. S. Hayase, N. Kikuchi, K. Sekein, and S. Sasaki, "Proposal of 8-state per symbol (binary ASK and QPSK) 30-Gbit/s optical modulation/demodulation scheme," in *European Conference on Optical Communication* (Institute of Electrical Engineers, 2003), paper TH2.6.4.
5. C. Kim and G. Li, "Direct-detection optical differential 8-level phase-shift keying (OD8PSK) for spectrally efficient transmission," Opt. Express **12**, 3415–3421 (2004).
6. Y. Han, C. Kim, and G. Li, "Simplified receiver implementation for optical differential 8-level phase-shift keying," Electron. Lett. **40**, 1372–1373 (2004).
7. Y. Han and G. Li, "Direct detection differential polarization-phase-shift keying based on Jones vector," Opt. Express **12**, 5821–5826 (2004).
8. L. G. Kazovsky, S. Benedetto, and A. E. Willner, *Optical Fiber Communication Systems* (Artech House, 1996).
9. T. Okoshi and K. Kikuchi, *Coherent Optical Fiber Communications* (Springer, 1988).
10. R. Noe, D. Sandel, M. Yoshida-Dierolf, S. Hinz, V. Mirvoda, A. Schopflin, C. Glingener, E. Gottwald, C. Scheerer, G. Fischer, T. Weyrauch, and W. Haase, "Polarization mode dispersion compensation at 10, 20, and 40 Gb/s with various optical equalizers," J. Lightwave Technol. **17**, 1602–1616 (1999).
11. J. R. Barry and J. M. Kahn, "Carrier synchronization for homodyne and heterodyne-detection of optical quadriphase-shift keying," J. Lightwave Technol. **10**, 1939–1951 (1992).

12. L. Kazovsky, "Balanced phase-locked loops for optical homodyne receivers: performance analysis, design considerations, and laser linewidth requirements," J. Lightwave Technol. **4**, 182–195 (1986).
13. K. Kikuchi, "Phase-diversity homodyne detection of multilevel optical modulation with digital carrier phase estimation," IEEE J. Sel. Top. Quantum Electron. **12**, 563–570 (2006).
14. G. Goldfarb and G. Li, "BER estimation of QPSK homodyne detection with carrier phase estimation using digital signal processing," Opt. Express **14**, 8043–8053 (2006).
15. R. Noe, "PLL-free synchronous QPSK polarization multiplex/diversity receiver concept with digital I&Q baseband processing," IEEE Photon. Technol. Lett. **17**, 887–889 (2005).
16. R. Noé, "PLL-Free synchronous QPSK receiver concept with digital I&Q baseband processing," in *Proceedings of the 30th European Conference on Optical Communication (ECOC)* (2004), paper We4. P.120.
17. D. S. Ly-Gagnon, S. Tsukarnoto, K. Katoh, and K. Kikuchi, "Coherent detection of optical quadrature phase-shift keying signals with carrier phase estimation," J. Lightwave Technol. **24**, 12–21 (2006).
18. R. Noe, "Phase noise-tolerant synchronous QPSK/BPSK baseband-type intradyne receiver concept with feedforward carrier recovery," J. Lightwave Technol. **23**, 802–808 (2005).
19. J. G. Proakis and D. G. Manolakis, *Digital Signal Processing: Principles, Algorithms, and Applications* (Prentice Hall, 1996).
20. M. G. Taylor, "Phase estimation methods for optical coherent detection using digital signal processing," J. Lightwave Technol. (to be published).
21. A. Leven, N. Kaneda, U.-V. Koc, and Y.-K. Chen, "Frequency estimation in intradyne reception," IEEE Photon. Technol. Lett. **19**, 366–368 (2007).
22. E. Ip and J. M. Kahn, "Feedforward carrier recovery for coherent optical communications," J. Lightwave Technol. **25**, 2675–2692 (2007).
23. Y. Han and G. Li, "Coherent optical communication using polarization multiple-input-multiple-output," Opt. Express **13**, 7527–7534 (2005).
24. D. Gesbert, M. Shafi, S. Da-shan, P. J. Smith, and A. Naguib, "From theory to practice: an overview of MIMO space-time coded wireless systems," IEEE J. Sel. Areas Commun. **21**, 281–302 (2003).
25. A. H. Sayed, *Fundamentals of Adaptive Filtering* (Wiley, 2003).
26. S. J. Savory, G. Gavioli, R. I. Killey, and P. Bayvel, "Electronic compensation of chromatic dispersion using a digital coherent receiver," Opt. Express **15**, 2120–2126 (2007).
27. D. Godard, "Self-recovering equalization and carrier tracking in two-dimensional data communication systems," IEEE Trans. Commun. **28**, 1867–1875 (1980).
28. M. G. Taylor, "Coherent detection method using DSP for demodulation of signal and subsequent equalization of propagation impairments," IEEE Photon. Technol. Lett. **16**, 674–676 (2004).
29. G. Goldfarb and G. Li, "Chromatic dispersion compensation using digital IIR filtering with coherent detection," IEEE Photon. Technol. Lett. **19**, 969–971 (2007).
30. E. Ip and J. M. Kahn, "Digital equalization of chromatic dispersion and polarization mode dispersion," J. Lightwave Technol. **25**, 2033–2043 (2007).
31. S. Tsukamoto, K. Katoh, and K. Kikuchi, "Unrepeated 20-Gbits/s QPSK

transmission over 200-km Standard single-mode fiber using homodyne detection and DSP for dispersion compensation," in *Optical Fiber Communication Conference and Exposition and The National Fiber Optic Engineers Conference*, Technical Digest (CD) (Optical Society of America, 2006), paper OWB4.
32. R. I. Killey, P. M. Watts, V. Mikhailov, M. Glick, and P. Bayvel, "Electronic dispersion compensation by signal predistortion using digital processing and a dual-drive Mach–Zehnder modulator," IEEE Photon. Technol. Lett. **17**, 714–716 (2005).
33. S. L. Woodward, H. Sun-Yuan, M. D. Feuer, and M. Boroditsky, "Demonstration of an electronic dispersion compensator in a 100-km10-Gb/s ring network," IEEE Photon. Technol. Lett. **15**, 867–869 (2003).
34. K. Roberts, L. Chuandong, L. Strawczynski, M. O. Sullivan, and I. Hardcastle, "Electronic precompensation of optical nonlinearity," IEEE Photon. Technol. Lett. **18**, 403–405 (2006).
35. E. Yamazaki, F. Inuzuka, K. Yonenaga, A. Takada, and M. Koga, "Compensation of interchannel crosstalk induced by optical fiber nonlinearity in carrier phase-locked WDM system," IEEE Photon. Technol. Lett. **19**, 9–11 (2007).
36. R.-J. Essiambre, P. J. Winzer, X. Q. Wang, W. Lee, C. A. White, and E. C. Burrows, "Electronic predistortion and fiber nonlinearity," IEEE Photon. Technol. Lett. **18**, 1804–1806 (2006).
37. K. Kikuchi, "Phase-diversity homodyne detection of multilevel optical modulation with digital carrier phase estimation," IEEE J. Sel. Top. Quantum Electron. **12**, 563–570 (2006).
38. X. Li, X. Chen, G. Goldfarb, E. Mateo, I. Kim, F. Yaman, and G. Li, "Electronic post-compensation of WDM transmission impairments using coherent detection and digital signal processing," Opt. Express **16**, 880–888 (2008).
39. C. Xu and X. Liu, "Postnonlinearity compensation with data-driven phase modulators in phase-shift keying transmission," Opt. Lett. **27**, 1619–1621 (2002).
40. G. P. Agrawal, *Nonlinear Fiber Optics*, 4th ed. (Academic, 2006).
41. L. Xun, C. Xingzhong, and M. Qasmi, "A broad-band digital filtering approach for time-domain simulation of pulse propagation in optical fiber," J. Lightwave Technol. **23**, 864–875 (2005).
42. G. P. Agrawal, *Nonlinear Fiber Optics*, 2nd ed. (Academic, 1995).
43. E. Mateo, L. Zhu, and G. Li, "Impact of XPM and FWM on the digital implementation of impairment compensation for WDM transmission using backward propagation," Opt. Express **16**, 16124–16137 (2008).
44. T. Schneider, *Nonlinear Optics in Telecommunications* (Springer, 2004).
45. G. Goldfarb, M. G. Taylor, and G. Li, "Experimental demonstration of fiber impairment compensation using the split-step finite-impulse-response filtering method," IEEE Photon. Technol. Lett. **20**, 1887–1889 (2008).
46. G. Goldfarb, G. Li, and M. G. Taylor, "Orthogonal wavelength-division multiplexing using coherent detection," IEEE Photon. Technol. Lett. **19**, 2015–2017 (2007).
47. C. Francia, "Constant step-size analysis in numerical simulation for correct four-wave-mixing power evaluation in optical fiber transmission systems," IEEE Photon. Technol. Lett. **11**, 69–71 (1999).
48. X. Zhou, J. Yu, D. Qian, T. Wang, G. Zhang, and P. Magill, "8 × 114 Gb/s,

25-GHz-spaced, PolMux-RZ-8PSK transmission over 640 km of SSMF employing digital coherent detection and EDFA-only amplification," in *Optical Fiber Communication Conference and Exposition and The National Fiber Optic Engineers Conference*, OSA Technical Digest (CD) (Optical Society of America, 2008), paper PDP1.
49. M. Seimetz, L. Molle, D.-D. Gross, B. Auth, and R. Freund, "Coherent RZ-8PSK transmission at 30 Gbits/s over 1200 km employing homodyne detection with digital carrier phase estimation," in *Proceedings of the 33rd European Conference on Optical Communication (ECOC)* (2007), paper WE 08.03.04.
50. H. Sun, K. T. Wu, and K. Roberts, "Real-time measurements of a 40 Gb/s coherent system," Opt. Express **16**, 873–879 (2008).
51. M. Yoshida, H. Goto, K. Kasai, and M. Nakazawa, "64 and 128 coherent QAM optical transmission over 150 km using frequency-stabilized laser and heterodyne PLL detection," Opt. Express **16**, 829–840 (2008).
52. A. D. Ellis and F. C. G. Gunning, "Spectral density enhancement using coherent WDM," IEEE Photon. Technol. Lett. **17**, 504–506 (2005).
53. W. Shieh, H. Bao, and Y. Tang, "Coherent optical OFDM: theory and design," Opt. Express **16**, 841–859 (2008).
54. W. Shieh, X. W. Yi, Y. Ma, and Q. Yang, "Coherent optical OFDM: has its time come? [Invited]," J. Opt. Netw. **7**, 234–255 (2008).
55. A. J. Lowery and J. Armstrong, "Orthogonal-frequency-division multiplexing for dispersion compensation of long-haul optical systems," Opt. Express **14**, 2079–2084 (2006).
56. A. J. Lowery, L. B. Du, and J. Armstrong, "Performance of optical OFDM in ultralong-haul WDM lightwave systems," J. Lightwave Technol. **25**, 131–138 (2007).
57. I. Kim, C. Kim, and G. Li, "Requirements for the sampling source in coherent linear sampling," Opt. Express **12**, 2723–2730 (2004).
58. X. Chen, I. Kim, G. Li, H. Zhang, and B. Zhou, "Coherent detection using optical time-domain sampling," in *Optical Fiber Communication Conference and Exposition and The National Fiber Optic Engineers Conference*, OSA Technical Digest (CD) (Optical Society of America, 2008), paper JThA62.
59. K. Kikuchi, K. Igarashi, Y. Mori, and C. Zhang, "Demodulation of 320-Gbits/s optical quadrature phase-shift keying signal with digital coherent receiver having time-division demultiplexing function," in *Optical Fiber Communication Conference and Exposition and The National Fiber Optic Engineers Conference*, OSA Technical Digest (CD) (Optical Society of America, 2008), paper OTuO4.
60. T. Pfau, S. Hoffmann, R. Peveling, S. Bhandare, S. K. Ibrahim, O. Adamczyk, M. Porrmann, R. Noe, and Y. Achiam, "First real-time data recovery for synchronous QPSK transmission with standard DFB lasers," IEEE Photon. Technol. Lett. **18**, 1907–1909 (2006).
61. T. Pfau, S. Hoffmann, O. Adamczyk, R. Peveling, V. Herath, M. Porrmann, and R. Noe, "Coherent optical communication: towards realtime systems at 40 Gbits/s and beyond," Opt. Express **16**, 866–872 (2008).
62. P. P. Mitra and J. B. Stark, "Nonlinear limits to the information capacity of optical fibre communications," Nature **411**, 1027–1030 (2001).